NF-κB-Inducing Kinase Maintains Mitochondrial Efficiency and Systemic Metabolic Homeostasis

Authors: Kathryn M. Pflug[1, 2], Dong W. Lee[1], Justin Keeney[1], Raquel Sitcheran[1, 2, *]

Affiliations:

[1] Department of Molecular & Cellular Medicine, Texas A&M University Health Science Center, College Station TX 77845, USA

[2] Interdisciplinary Graduate Program in Genetics, Texas A&M University, College Station TX 77845, USA

* Correspondence: sitcheran@tamu.edu

Conflicts of Interest: The authors declare no conflicts of interest.

Keywords

NF-κB-inducing kinase, Glycolysis, Oxidative Phosphorylation (OXPHOS), Spare Respiratory Capacity, Proton Leak, High-Fat Diet

Abstract

Background: NF-κB-inducing kinase (NIK) is a critical regulator of immunity and inflammation and NIK loss-of-function mutations have recently been described in patients with primary immunodeficiency disease. Based on our previous work showing that NIK regulates adaptive metabolic responses in glucose-starved cancer cells, we investigated whether NIK is required for mitochondrial functions in bioenergetic processes and metabolic responses to nutritional stress in NIK knockout (KO) mice, which recapitulate the clinical presentation of NIK PID patients.

Methods: We performed whole body composition analysis of wild type (WT) and NIK KO mice using EchoMRI and DEXA imaging. Seahorse extracellular flux analyses were used to monitor oxidative phosphorylation and glycolysis through oxygen consumption rates (OCR) and extracellular acidification rates (ECAR) in preadipocyte cells and in ex vivo adipose tissue. NIK regulation of systemic metabolic output was measured by indirect calorimetry using TSE Phenomaster metabolic chambers under basal conditions as well as in response to nutritional stress induced by a prolonged high-fat diet (HFD). Finally, we analyzed a role for NIK in adipocyte differentiation, as well as the contributions of canonical and noncanonical NF-κB signaling to adipose development and metabolic output.

Results: We observed that in adipose cells, NIK is required for maintaining efficient mitochondrial membrane potential and spare respiratory capacity (SRC), indicators of mitochondrial fitness. NIK KO preadipocytes and ex vivo adipose tissue exhibited diminished SRC, increased proton leak, with compensatory upregulation of glycolysis. Systemically, NIK KO mice exhibited increased glucose utilization, increased energy expenditure, and reduced adiposity, which persisted under the stress of HFD. Finally, while NIK controlled adipocyte differentiation through activation of RelB and the noncanonical NF-κB pathway, NIK regulation of metabolism in preadipocytes was NF-κB/RelB-independent.

Conclusion: Our results demonstrate that NIK is required for metabolic homeostasis both locally, on a cellular and tissue level, as well as systemically, on an organismal level. Collectively, the data suggest that NIK KO cells upregulate glycolytic metabolism as a compensatory response to impaired mitochondrial fitness (diminished SRC) and mitochondrial efficiency (increased proton leak). To meet changes in bioenergetic demands, NIK KO mice undergo metabolic rewiring through increased glucose utilization and glycolysis, which persists under the stress of overnutrition with a HFD. Moreover, while NIK regulation of metabolism is RelB-independent, NIK regulation of adipocyte development requires RelB and activation of the noncanonical NF-κB pathway. Our findings establish NIK as an important regulator of cellular and systemic metabolic homeostasis, suggesting that metabolic dysfunction may be an important component of primary immunodeficiency diseases arising from loss of NIK function.

Abbreviations: NIK- NF-κB-Inducing Kinase, NF-κB- Nuclear factor kappa light chain enhancer of activated B cells, IKKα- inhibitor of kappa B kinase alpha, PID- primary immunodeficiency, SRC- spare respiratory capacity, OCR- oxygen consumption rate, ECAR- extracellular acidification rate, ingWAT- inguinal white adipose tissue, DEXA- dual energy X-ray absorptiometry, gWAT- gonadal white adipose tissue, RER- respiratory exchange rate, HFD- High-fat diet, PPARγ- peroxisome proliferator activated receptor, C/EBPα- CCAAT enhancer binding protein alpha, ETYA- eicosatetraynoic acid, TNFα- tumor necrosis factor alpha, TWEAK- tumor necrosis factor weak like.

1. Introduction

Nuclear Factor-κB (NF-κB)-inducing kinase (NIK), encoded by *MAP3K14*, is a serine, threonine protein kinase that that is best known for its function as an upstream inducer of NF-κB signaling to regulate innate and adaptive immunity. While NIK can activate canonical and noncanonical NF-κB pathways, it is uniquely required for activation of noncanonical NF-κB signaling through phosphorylation of Inhibitor of κB Kinase α (IKKα), which triggers p100 processing to p52, and generation of transcriptionally active p52-RelB NF-κB complexes [1–4]. NIK has critical roles in B-cell, lymphocyte, and lymph node development, immunoglobulin (Ig) production and T-cell function. Consequently, Nik^{aly} mutant mice (*aly*; alymphoplasia), which lack NIK activity, and NIK knockout mice (NIK KO) exhibit lymphopenia, abnormal Peyer's patches, aberrant splenic and thymic structures, reduced B-cell numbers and Ig serum levels leading to humoral immunodeficiency [1,5–9]. In humans, NIK loss-of-function mutations were recently identified in patients with primary immunodeficiency (PID) who exhibit similar immune defects as Nik^{aly} and NIK KO mice [10,11], demonstrating the relevance of NIK deficient mouse models for immunodeficiency disease.

We, and others, have elucidated important NF-κB-independent metabolic functions for NIK, including roles in mitochondrial dynamics, metabolic reprogramming in macrophages and under nutrient stress in cancer cells, as well as regulation of glycolysis in T-cells [12–15]. In response to diet-induced obesity, gain-of-function studies have shown that NIK induces hyperglycemia by increasing glucagon activity, and liver steatosis through induction of fatty acid oxidation, and loss of NIK was shown to increase glucose and insulin tolerance [16–18]. Our recent work has established NIK mitochondrial localization and regulation of mitochondrial respiration and fitness, promoting metabolic adaptation of cancer cells to glucose starvation [15]. However, NIK regulation of mitochondrial metabolism has not been examined in adipose tissue, or on an organismal level.

93 Metabolic homeostasis relies on a balance between inputs such as glucose and oxygen
94 necessary for energetic processes and utilization of catabolic pathways involving glycolysis and
95 oxidative phosphorylation (OXPHOS) for efficient energy production [19,20]. Utilization of these
96 major metabolic pathways is dynamic and shifts in response to alterations in cellular states or
97 stress [21,22]. Glycolysis and OXPHOS are interwoven and dysregulation in one can alter the
98 flux or rate of the other [23–25]. Although glycolysis yields low amounts of ATP, it is important for
99 feeding into the TCA cycle and electron transport chain (ETC) for rapid production of ATP,
100 particularly under low oxygen availability [26–28]. Furthermore, glucose catabolism is preferred
101 in response to stress as it requires the lowest input of ATP [29–31]. Oxidative phosphorylation, or
102 aerobic respiration, is more commonly utilized to meet ATP demands. Important for mitochondrial
103 respiration is its spare respiratory capacity (SRC), a measurable indicator of mitochondrial fitness,
104 or the ability to upregulate oxygen consumption and ATP production to meet changes in energetic
105 demand [32–34]. Energy derived from mitochondria is essential for maintaining cellular
106 homeostasis, as well as in response to stress. Reciprocally, on an organismal level, alterations in
107 mitochondrial functions impact physiological and behavioral responses, as seen in individuals
108 with impaired ETC function due to primary mitochondrial disorders (PMDs), who are unable to
109 adapt to dietary and physiological stressors [35,36]. As such, mitochondrial fitness and efficiency
110 is essential to organismal homeostasis and adaptation to bioenergetic stress.

111 Here we investigate a functional and developmental role for NIK in controlling metabolic
112 homeostasis basally and in response to nutritional stress induced by a high-fat diet (HFD). Our
113 data demonstrate that NIK deficient preadipocytes and *ex vivo* tissue exhibited loss of
114 mitochondrial SRC and increased proton leak. This uncoupling of mitochondrial respiration and
115 inefficient metabolism was accompanied by a compensatory increase in glycolysis and
116 extracellular acidification rate (ECAR). Furthermore, we show that NIK regulation of mitochondrial
117 SRC and proton leak is independent of noncanonical RelB/NF-κB signaling. Similar to NIK KO

118 cells and tissue, NIK deficiency in mice resulted in increased glucose utilization and glycolysis to
119 meet energetic demands. In NIK KO mice, and *ex vivo* adipose tissue, this increased energy
120 expenditure resulted in reduced adiposity and resistance to adipose accumulation and weight
121 gain through development, as well as under a HFD. While NIK regulates mitochondrial functions
122 independently of RelB/NF-κB, we found that NIK promotes adipocyte differentiation in a
123 noncanonical NF-κB-dependent manner through transcriptional regulation of key adipogenic
124 transcription factors. These results are the first to describe NIK regulation of adiposity through
125 NF-κB-dependent development signaling, as well as NF-κB-independent regulation of local-
126 tissue metabolism and systemic energy expenditure, suggesting that systemic mitochondrial
127 metabolic defects are an underlying component of immune dysfunction.

128

129 **2. Results**

130 **2.1 NIK KO mice have reduced adiposity**

131 Whole body composition analyses were performed using dual-energy x-ray
132 absorptiometry (DEXA) imaging to evaluate potential alterations in systemic body composition
133 due to NIK deficiency. Mice were utilized between the ages of 2-4 months, that exhibited a healthy
134 deposition. We observed that NIK KO mice displayed a significant reduction in overall fat mass
135 and considerably smaller visceral and subcutaneous adipose tissue depots (Figure 1A). Further
136 assessment of whole body composition using EchoMRI™, demonstrated that both NIK KO males
137 and females had a significant reduction in overall fat mass and a higher lean mass ratio relative
138 to body weight (Figure 1B,C). Visceral gonadal white adipose tissue (gWAT) depots were
139 substantially reduced in male and female NIK KO mice compared to WT and HET mice (Figure
140 1D,E, Supp. Figure 1A). Similarly, subcutaneous inguinal white adipose tissue (ingWAT) was
141 reduced in NIK KO mice (Supp. Figure 1B). While WT mice increased in fat mass as they aged
142 from 2 to 4 months, NIK KO mice maintained a reduced fat mass during this time period (Figure

143 1F, Supp. Figure 1C,D), and exhibited no signs of infection. Although NIK KO mice gained less
144 fat, this was not due to behavioral changes as they consumed more food and water with reduced
145 physical activity than their WT littermates (Supp. Figure 1C,D). Furthermore, though a reduction
146 in adiposity was notable even at 2 months age (Supp. Fig. 1F), NIK KO mice did not significantly
147 differ in weight compared to WT mice until 15 weeks of age in males, possibly when the rate of
148 fat mass development in WT mice surpassed the rate of body growth and adipose development
149 in NIK KO mice (Supp. Figure 1G,H). Oil Red O staining of liver sections revealed no differences
150 in exogenous liver lipid accumulation between WT and NIK KO mice (Supp. Figure 1I), which can
151 occur due to defects in adipocyte function and lipolysis [37,38], suggesting a role for NIK in the
152 adipose tissue development.
153

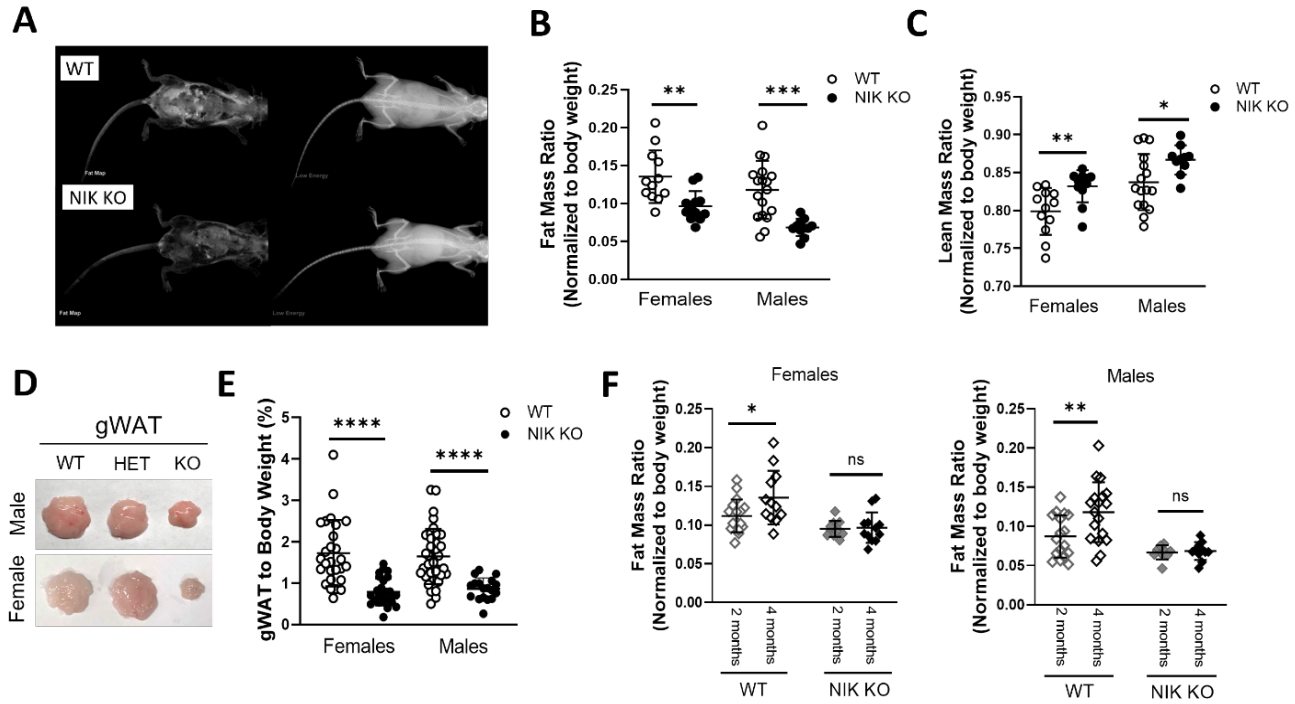

154

155 **Figure 1: NIK KO mice have reduced adiposity**

156 **(A)** DEXA scans of chow fed male WT and NIK KO mice at 2 months, displaying overall fat map
157 (left) and overall low energy map (right). **(B)** EchoMRI^{TM} measurements of overall fat and **(C)** lean

158 mass of male and female mice normalized to body weight. WT n= 12 females and 18 males, KO
159 n=12 females and 11 males. **(D)** Gonadal adipose tissue from male or female mice. **(E)** Weight
160 of gonadal fat between WT and NIK KO male and female mice normalized to body weight. WT
161 n= 27 females and 36 males, KO n= 26 females and 18 males. **(F)** Fat mass ratio from body
162 composition data of female and male WT and NIK KO mice at 2 and 4 months of age. At 2-
163 months-old WT n=17 females and 17 males, KO n= 9 females and 9 males. At 4-months-old WT
164 n= 12 females and 18 males, KO n= 12 females and 11 males. **(B-C,E-F)** Data represented as
165 mean ± SD, Unpaired Student t-test.

166

167 **2.2 NIK regulates mitochondrial respiration and efficiency**

168 We previously demonstrated that NIK localizes to mitochondria, promoting mitochondrial
169 fission and oxidative metabolism in glioblastoma cells [13]. Similarly, we observed that multipotent
170 C3H10T1/2 cells, capable of differentiating into adipocytes, also exhibited larger, more fused
171 mitochondria when NIK expression was ablated. Exogenous expression of human NIK in NIK KO
172 cells (NIK KO-hNIK) restored mitochondrial morphology similar to that observed in WT cells
173 (Figure 2A,B). Similarly, 3T3-L1 NIK KO preadipocytes also exhibited a fused mitochondria
174 phenotype. However, cells lacking the downstream noncanonical NF-κB transcription factor, RelB
175 (RelB KO cells), did not exhibit a fused mitochondrial morphology similar to NIK KO cells,
176 suggesting this phenotype in is NIK-dependent (Figure 2C). Given the reduction in adiposity and
177 changes in mitochondria morphology in NIK KO cells, we sought to determine whether NIK
178 regulates mitochondrial function in adipocytes. Metabolic analysis of 3T3-L1 cells by Seahorse
179 extracellular flux assay revealed that NIK KO cells exhibited higher basal oxygen consumption
180 rate (OCR) but with significantly impaired mitochondrial spare respiratory capacity (SRC), and
181 increased mitochondrial proton leak, characteristic of inefficient mitochondrial metabolism (Figure
182 2D). Normal SRC and proton leak phenotypes were restored in NIK KO-hNIK cells (Figure 2D,

183 Supp. Fig 1J), demonstrating that the aberrant mitochondrial metabolism is NIK-dependent. RelB
184 KO cells did not have impaired SRC and proton leak, showing that NIK regulation of mitochondrial
185 efficiency is also noncanonical NF-κB-independent (Figure 2D). NIK KO and NIK KO-hNIK cells
186 also showed an increase in basal extracellular acidification rate (ECAR), a readout for glycolysis,
187 while RelB KO cell ECAR was similar to WT (Figure 2E), consistent with NF-κB-independent roles
188 for NIK in adipocyte metabolism. Basally, NIK KO, NIK KO-hNIK and RelB KO cells had similar
189 basal energetic profiles compared with WT cells. However, NIK KO cells exhibited impaired OCR
190 in response to mitochondrial stressors, which was accompanied by a compensatory increase in
191 glycolysis, whereas RelB KO cell metabolism was unaffected (Figure 2F). Exogenous NIK
192 expression rescued OCR elevation under a stressed state in NIK KO cells, demonstrating a
193 requirement for NIK to meet metabolic demand in a stressed state through OXPHOS (Figure 2G).

194

195

196

197

198

199

200

201

202

203

204

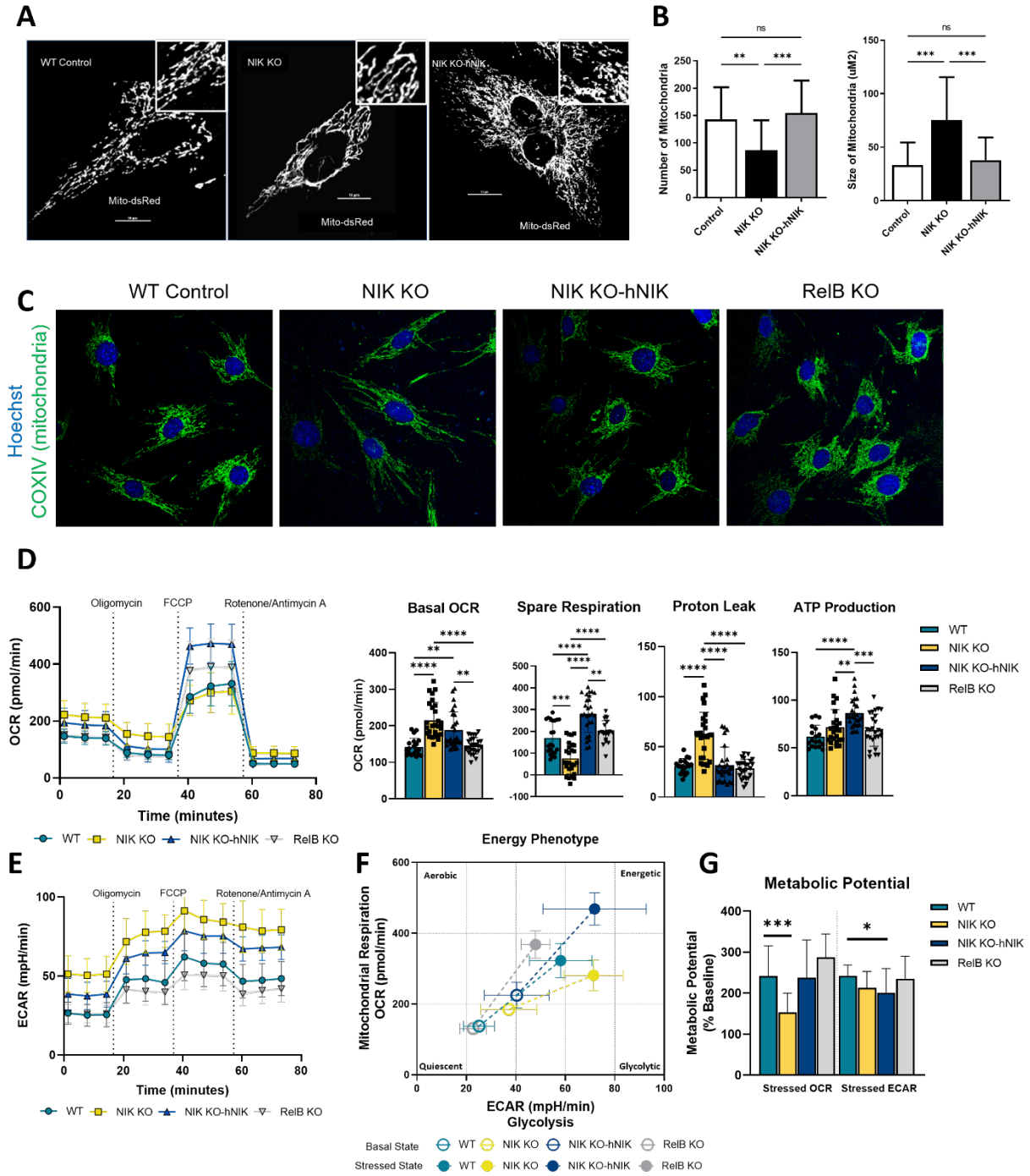

Figure 2: NIK regulates mitochondrial respiration and efficiency

(A) Representative imaging of C3H10T1/2, mouse stem cells, transfected with Mito-dsRed. **(B)** Image J quantification of Mito-dsRed transfected WT, NIK KO, and NIK KO-hNIK C3H10T1/2 cells. Data represented as mean ± SD, One-Way ANOVA **(C)** Immunofluorescence imaging of

210 WT, NIK KO, NIK KO-hNIK, and RelB KO C3H10T1/2 cells with mitochondria (COXIV, green)
211 and nuclear (Hoechst, blue) staining. **(D)** Seahorse extracellular flux analysis of 3T3-L1
212 preadipocytes oxidative stress test (mitochondria stress test) displaying oxygen consumption
213 rate (OCR) (statistics compared to WT) and **(E)** extracellular acidification rate (ECAR). **(D-E)**
214 OCR and ECAR line graphs are represented as mean ± SEM. Mitochondria stress test dot plots
215 are represented as mean ± SD, One-Way ANOVA. N= 4 independent, biological replicates with
216 5-8 technical replicates per independent run. **(F)** Cell energy phenotype of 3T3-L1 cells from
217 seahorse analysis showing basal states of cell (open square) by OCR and ECAR to stressed
218 states (closed square). Data represented as mean ± SD. **(G)** Metabolic potential of 3T3-L1 cells
219 from seahorse analysis with contribution by either OXPHOS (OCR) or by glycolysis (ECAR)
220 after FCCP injection (stressed rates). Data represented as mean ± SD, One-Way ANOVA**. (F-**
221 **G**). N= 3 independent, biological replicates with 5-8 technical replicates per independent run.

222

223

224

225 **2.3 Glycolytic dependence increases in response to metabolic demand in NIK KO adipose**
226 **tissue**

227 To evaluate whether NIK regulates adipocyte metabolism in the context of its native
228 microenvironment, we analyzed OCR and ECAR in *ex vivo* adipose tissue from WT and NIK KO
229 mice. Although basal OCR was not significantly altered, NIK KO ingWAT and gWAT depots
230 exhibited impaired maximal respiration and reduced SRC, increased proton leak and decreased
231 ATP production, similar to adipocyte cells (Figure 3A). We also observed robustly elevated ECAR
232 in both NIK KO adipose depots, consistent with metabolic reprogramming to meet energetic
233 demands and compensate for inefficient OXPHOS (Figure 3B). Both adipose depots were able

234 to increase glycerol levels in response to isoproterenol, a β-agonist and lipolytic stimulant,
235 suggesting that NIK KO adipose tissues are functional, with gWAT displaying enhanced lipid
236 turnover compared to WT (Figure 3C). Together, these findings suggest that loss of NIK in
237 adipocytes and adipose tissue resulted in mitochondrial dysfunction exhibited by impaired SRC
238 and elevated proton leak, causing an increase in energetic demand that is met by enhanced
239 glycolytic metabolism.

240

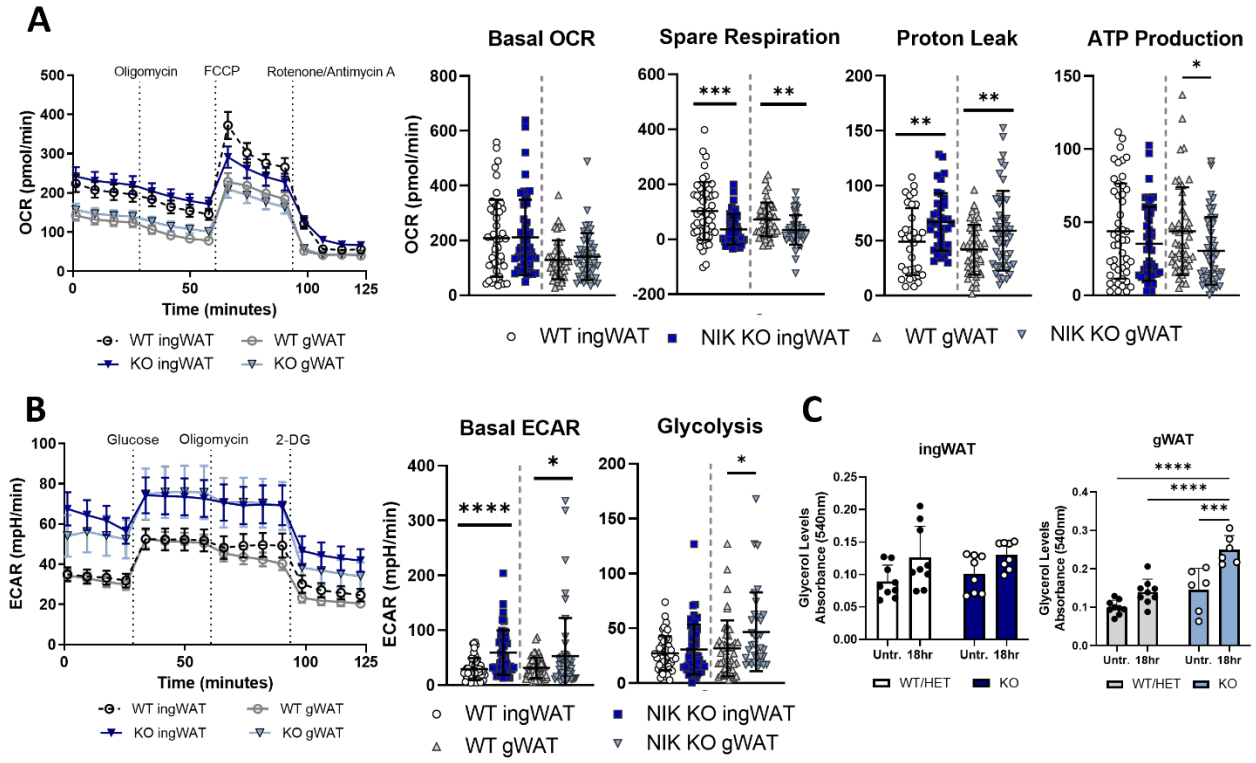

241

242

243 **Figure 3: Glycolytic dependence increases in response to metabolic demand in NIK KO**
244 **mice**

245 **(A)** Seahorse extracellular flux analysis of *ex vivo* mouse gonadal (gWAT) or inguinal WAT
246 (ingWAT) with an oxidative stress test (Mitochondria Stress Test). **(B)** Seahorse extracellular flux

247 analysis of *ex vivo* mouse gonadal or inguinal WAT with Glycolysis Stress Test. **(A-B)** Data
248 represented as mean ± SEM for line graphs and mean ± SD for dot plots. WT n=4 females and 5
249 males, KO n= 4 females and 3 males. Data normalized by protein. **(C)** Glycerol levels of gonadal
250 or inguinal WAT with lipolysis stimulated with isoproterenol and measured prior to treatment
251 (untreated) and after 18-hour incubation. Data represented as mean ± SD, Sidak's Multiple
252 Comparison Test. Data normalized by tissue weight.

253

254 **2.4 Sex dimorphic metabolic differences are exhibited in NIK KO mice**

255 We next sought to evaluate whether NIK-dependent metabolism observed in cellular and
256 adipose tissue impacted systemic metabolism. Using indirect calorimetry metabolic cages, whole
257 body analyses of WT and NIK KO mice were performed across light and dark cycles to analyze
258 respiratory rates and energy expenditure, along with feed and water intake as well as activity.
259 Overall, female NIK KO mice displayed higher oxygen consumption and carbon dioxide
260 production rate throughout both periods of the day compared to their WT counterparts, while NIK
261 KO male systemic metabolic rates were not significantly altered (Figure 4 A, B). By measuring
262 respiration exchange rates (RER), substrate utilization for oxidation can be estimated. Glucose
263 oxidation has the highest respiration exchange rate, followed by protein, and then lipid oxidation
264 [29]. Tracking changes in oxidation preference between inactive (light) and active (dark) cycles
265 by RER measurements revealed that at 2 months of age, both WT and NIK KO mice similarly
266 utilize lipid oxidation during their inactive states (Supp. Figure 2D). However, as NIK KO mice
267 age, glucose or protein utilization for oxidation increases during their inactive periods, similar to
268 RER in their active periods. In contrast, WT mice maintain lower RER in their inactive states,
269 indicative of lipid oxidation. During active periods, WT and NIK KO RER increase similarly at both
270 ages (Figure 4C). Moreover, NIK KO mice displayed a higher overall energy expenditure,
271 particularly in females compared with males (Figure 4D). In addition to increased metabolic

output, NIK KO mice also exhibited higher temperatures at 2 months of age (Figure 4E), and female mice maintained elevated temperatures at 4 months (Supp. Figure 2A). Consistent with increased temperature and energy expenditure, we observed higher brown adipose tissue in both female and male NIK KO mice (Figure 4F). While male and female mice displayed adipose specific increases in metabolism from *ex vivo* extracellular flux analysis, only female mice exhibited systemic differences on a chow diet. This trend for an overall increase in whole body metabolic activity in the NIK KO mice is observable in aging mice (Supp. Figure 2).

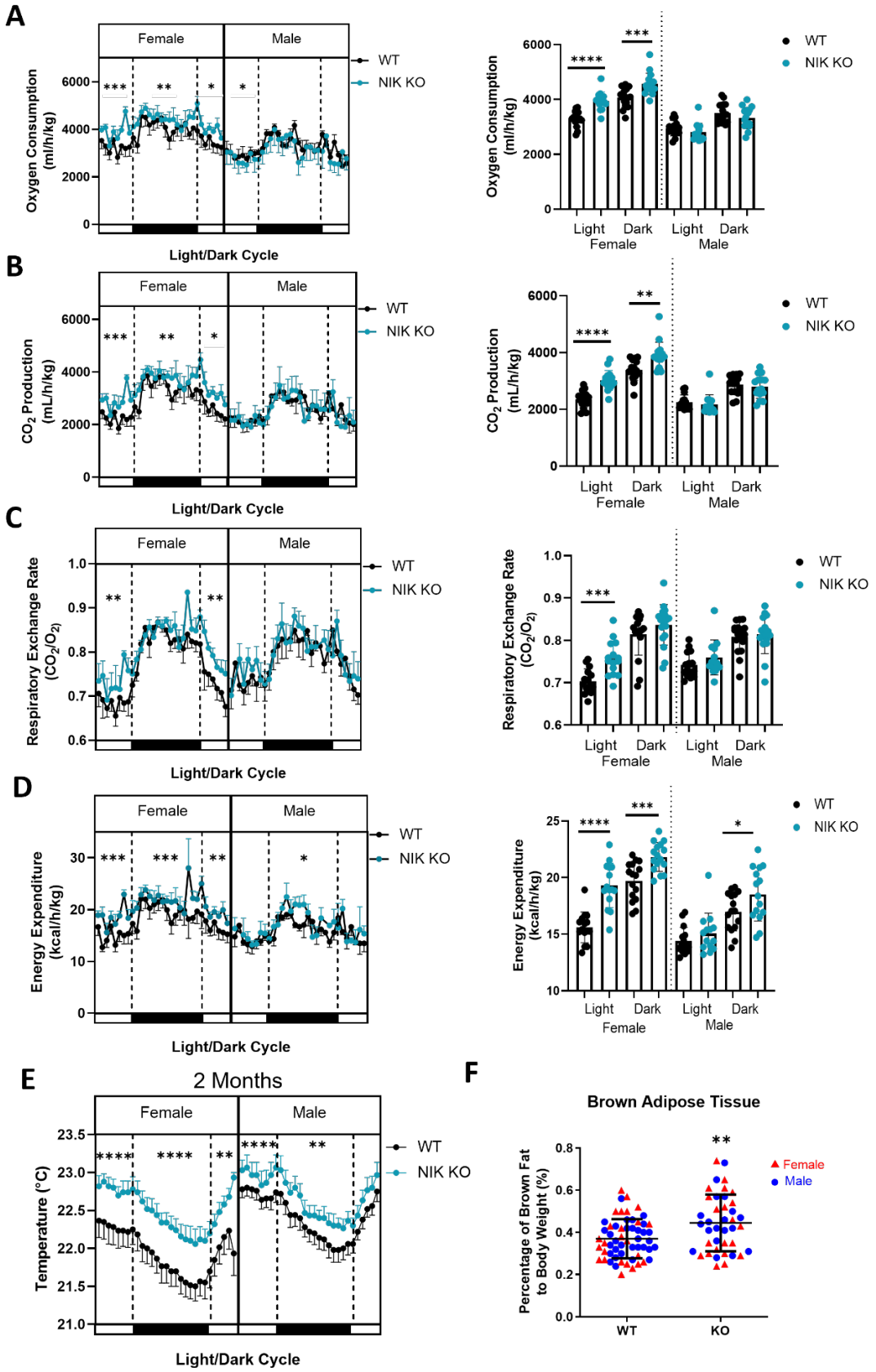
A
Female
Male
WT
NIK KO
Oxygen Consumption (ml/h/kg)
Light/Dark Cycle
Light
Dark
B
CO2 Production (mL/h/kg)
C
Respiratory Exchange Rate (CO2/O2)
D
Energy Expenditure (kcal/h/kg)
E
2 Months
Temperature (°C)
F
Brown Adipose Tissue
Percentage of Brown Fat to Body Weight (%)
Female
Male
WT
KO

293

294 **Figure 4: Sex dimorphic metabolic differences are exhibited in NIK KO mice**

295 **(A-D)** Systemic metabolic data collected from 4-month-old, chow fed male and female *Map3k14*
296 mice individually housed in TSE Phenomaster metabolic cages. Morning (light) and night (dark)
297 analysis from a 24-hour time period of **(A)** oxygen consumption, **(B)** CO_2 production, **(C)**
298 respiratory exchange rate (CO_2/O_2), and **(D)** caloric energy expenditure. **(E)** Metabolic cage
299 temperature with mice at 2 months of age. **(F)** Brown adipose tissue weights from male and
300 female, chow fed WT and NIK KO mice at 4 months of age. Data represented as mean ± SD
301 Males; WT n=25 females and 33 males, KO n=22 females and 19 males. Line graphs represented
302 as mean ± SEM, bar graphs represented as mean ± SD. **(A-D)** Females WT n=5 females and 4
303 males, KO n=6 females and 3 males. **(E)** WT n= 6 females and 5 males, KO n=5 females and 3
304 males. **(A-F)** Data analyzed by Unpaired Student t-test.

305

306

307 **2.5 NIK promotes adiposity in response to overnutrition with a high-fat diet**

308 Next, we investigated whether NIK plays a role in regulating systemic metabolism in
309 response to nutritional stress. After 2-3 months on a high-fat diet (HFD), both male and female
310 NIK KO mice exhibited significantly less weight gain than their WT counterparts (Figure 5A, B, C).
311 Whole body composition analysis by EchoMRI demonstrated that NIK KO mice maintained lower
312 fat mass and a higher lean mass ratio by body weight compared to WT mice (Figure 5D, E).
313 Overall, NIK KO mice gained about 3x less fat than WT mice on a HFD compared with standard
314 chow (Figure 5F). Analysis of individual adipose depots revealed that NIK KO mice on a HFD
315 exhibited a 50% decrease in gWAT tissue, along with a significant reduction in the subcutaneous
316 depot, ingWAT, compared to WT mice (Figure 5G,H). In addition to exhibiting reduced adiposity,
317 NIK KO mice were more efficient at clearing glucose from the blood in glucose tolerance tests

compared to WT littermates, suggesting an increase in insulin sensitivity (Figure 5I). Insulin tolerance testing confirmed this, demonstrating that NIK KO mice also cleared glucose more rapidly than WT mice after an administration of insulin (Figure 5J). Analysis of adipogenic gene expression from the inguinal WAT of HFD mice also revealed a reduction in fatty acid binding protein 4 (*FABP4*; Ap2), and an increase in GLUT4 and *GPD1* (Supp. Figure 3A,B), which is consistent with both an increase in glucose clearance of NIK KO mice and higher glycolytic demands of NIK KO adipose tissue. Moreover, glycogen synthase expression in the livers of NIK KO mice is decreased, suggesting reduced glucose storage compared to WT (Supp. Figure 3C,D). NIK KO mice on a HFD also exhibited reduced lipid levels in the liver compared to WT mice accompanied by lower gene expression of fatty acid binding protein (*FABP1*) and fatty acid oxidation genes (*MCAD, CPT1α*) (Supp. Figure 3D,E). Overall, these data demonstrated the critical role NIK has in facilitating adipose expansion and glucose homeostasis with overnutrition under a HFD.

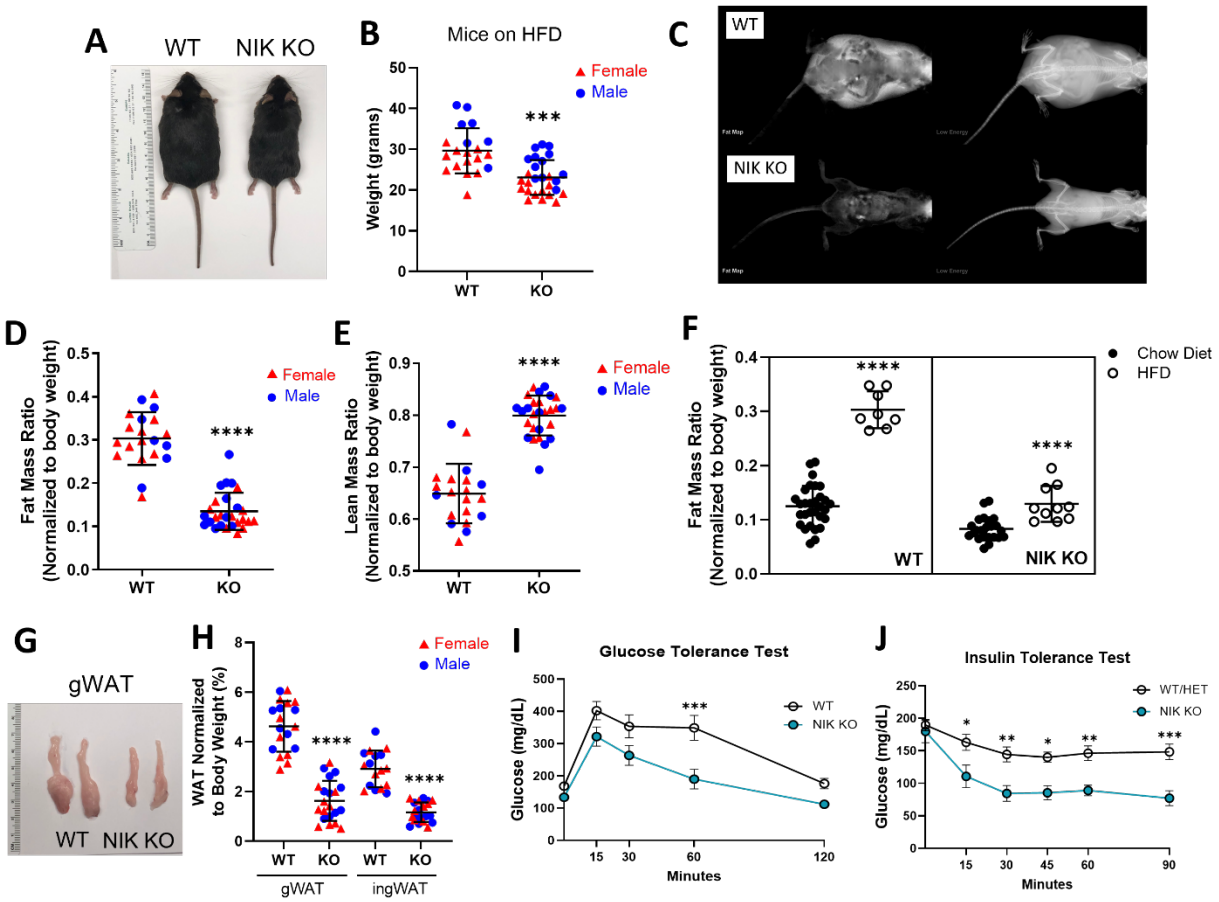

Figure 5: NIK promotes adiposity in response to overnutrition with a high-fat diet

(A) Images of male WT and NIK KO mice on HFD. **(B)** Weights of WT and NIK KO male and female mice exposed to a HFD for about 3 months (mice exposed to a HFD in utero up until weaning and then 8-10 weeks after weaning). Data represented as mean ± SEM, Unpaired Student t-test. **(C)** DEXA images of WT and NIK KO male mice on a HFD at about 3 months of age, displaying overall fat map (left) and overall low energy map (right). **(D)** EchoMRI^{TM} data of fat and **(E)** lean mass from female and male WT and NIK KO mice on a HFD normalized to weight. Data represented as mean ± SD, Unpaired Student t-test. **(F)** Fat mass data from EchoMRI^{TM} analysis comparing fat mass ratios from a chow diet to a HFD between WT and NIK KO mice. **(G)** Gonadal white adipose tissue from male mice on a HFD. **(H)** Weights of gonadal and inguinal

352 white adipose tissue from male and female mice normalized to body weight. Data represented as
353 mean ± SD, Unpaired Student t-test. **(I)** Glucose tolerance test on WT and NIK KO mice on a
354 HFD. Data represented at mean ± SEM, Sidak's Multiple Comparisons Test. WT n=8, NIK KO
355 n=12. **(J)** Insulin tolerance test on WT, HET and NIK KO mice on a HFD. Data represented at
356 mean ± SEM, Sidak's Multiple Comparisons Test. WT/HET n=10, NIK KO n=6.

357

358

359

360 **2.6 NIK is required for metabolic homeostasis in response to chronic dietary stress**

361 Extracellular flux analyses were then performed on *ex vivo* adipose tissue from mice
362 subjected to the chronic overnutrition with a HFD in utero through the age of 3 months. Adipose
363 tissue from NIK KO mice on a HFD showed a striking increase in basal OCR and ATP
364 production (Figure 6A). NIK KO ingWAT had significantly decreased SRC, while proton leak
365 was consistently increased in both NIK KO depots (Figure 6A), suggesting elevated, but
366 inefficient, mitochondrial metabolism, similar to results observed in NIK KO preadipocytes and
367 *ex vivo* NIK KO adipose tissue from chow-fed mice. Analysis of glycolytic metabolism also
368 demonstrated similar results to chow-fed mice, with NIK KO adipose tissue exhibiting
369 significantly higher basal ECAR rates and higher levels of glycolysis (Figure 6B). We also
370 observed elevated systemic metabolism in NIK KO mice on a HFD. Although we observed
371 some sex dimorphic metabolic dysregulation in NIK KO mice under a chow diet, with the chronic
372 stress of a HFD, both male and female NIK KO mice displayed elevated oxygen consumption
373 and CO_2 production (Supp. Fig. 4A,B) along with higher respiratory exchange rates, particularly
374 during the light cycle, or inactive period (Figure 6C, Supp. Fig 4C). Notably, robust increases in
375 energy expenditure and cage temperature were observed in NIK KO mice, demonstrating

376 considerably elevated metabolic output compared to WT mice at all times of the day with HFD
377 overnutrition (Figure 6D, Supp. Fig. 4D,E). Notably, leaner NIK KO mice did not exhibit
378 increased physical activity (Supp. Fig. 4F), or reduced water or feed intake (Supp. Fig. 4G,H).
379 Overall, our findings revealed that under either basal or nutrient stressed conditions NIK KO
380 mice exhibited elevated metabolism with higher energy expenditure but have inefficient
381 mitochondrial metabolism through impaired SRC and increased proton leak. Furthermore,
382 increased glycolysis and glucose utilization persisted to meet energetic demands under the
383 stress of a HFD, demonstrating an important role for NIK in metabolic homeostasis.

384

385

386

387

388

389

390

391

392

393

394

395

396

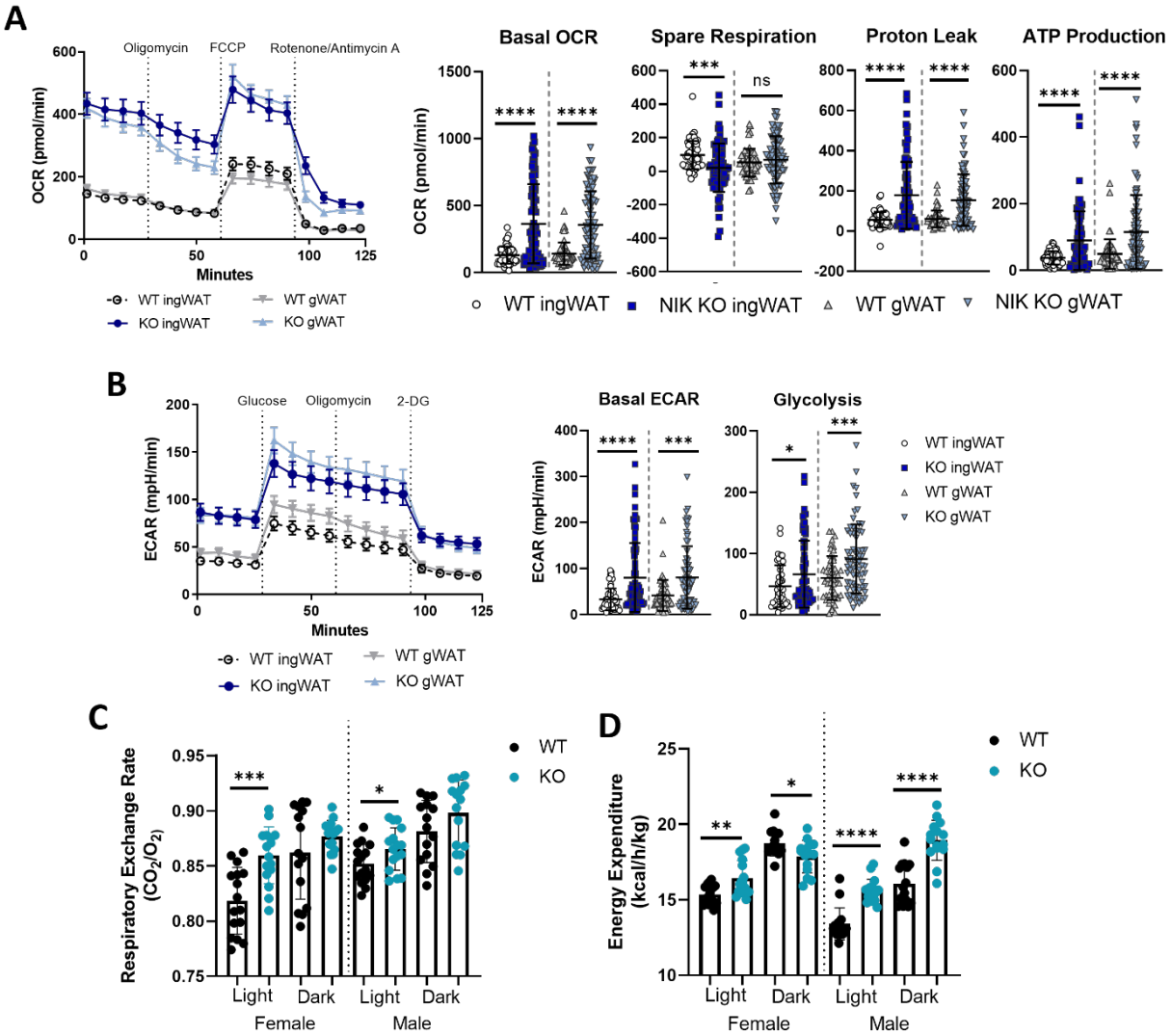

397

398 **Figure 6: NIK is required for metabolic homeostasis in response to chronic dietary stress**

399 **(A)** Seahorse extracellular flux analysis of *ex vivo* mouse gonadal or inguinal WAT with either
400 oxidative stress test (Mitochondria Stress Test) or with **(B)** Glycolysis Stress Test. **(A,B)** Data
401 represented as mean ± SEM for line graphs and mean ± SD for dot plots, Unpaired Student t-
402 test. WT n=4 females and 5 males , KO n=6 females and 7 males. **(C,D)** Indirect calorimetry
403 data collected from TSE Phenomaster cages of individually housed male and female *Map3k14*
404 mice on a HFD at about 3 months of age. Morning and night analysis from a 24-hour time period
405 of **(C)** respiratory exchange rate (CO_2/ O_2), and **(D)** caloric energy expenditure. WT n= 7

406 females and 5 males, KO n=8 females and 5 males. Data represented as mean ± SD, Unpaired
407 Student t-test.

408

409

410

411 **2.7 A role for noncanonical NF-κB-dependent signaling in promoting adiposity**

412 Given previous studies suggesting a role for NF-κB in adipocyte differentiation and
413 development, we investigated whether NIK-dependent noncanonical NF-κB activity was involved
414 in promoting adiposity. Compared to control cells, NIK KO C3H10T1/2 and 3T3-L1 cells were
415 severely impaired in their ability to form mature adipocytes, as demonstrated by staining of lipid
416 droplets. Expression of a wild-type human NIK construct in NIK KO cells (NIK KO-hNIK) restored
417 adipogenesis to the same extent as control cells (Figure 7A, Supp. Figure 5A,B). We also
418 observed that primary bone marrow-derived stem cells (MSCs) isolated from NIK KO mice were
419 impaired in their ability to differentiate into mature adipocytes compared to MSCs isolated from
420 WT mice (Supp. Figure 5C). Furthermore, treatment of WT C3H10T1/2 cells with a NIK-specific
421 inhibitor, B022, impeded adipocyte differentiation similar to cells lacking NIK (Supp. Figure 5D,E)
422 [39]. These results support a crucial, cell-intrinsic role for NIK in adipocyte development.

423 Next, we evaluated if NIK regulation of adipogenesis required downstream NF-κB
424 signaling. We observed that RelB KO 3T3-L1 cells exhibited impaired adipocyte differentiation
425 and overexpression of IKKα and RelB in NIK KO cells (NIK KO-IKKα, NIK KO-RelB) restored
426 adipocyte differentiation similar to NIK (NIK KO-hNIK). In contrast, overexpression of the
427 canonical NF-κB transcription factor RelA in NIK KO or RelB KO cells was unable to restore
428 adipocyte differentiation and RelA KO cells did not exhibit impaired adipogenesis (Figure 7B,
429 Supp. Figure 6A). Additionally, RelA phosphorylation at Ser536 (p-RelA-S536), a marker of its

430 transcriptional activation, decreased significantly 4-6 days after induction of adipocyte
431 differentiation. Conversely, expression of the noncanonical NF-κB protein RelB, increased
432 throughout adipocyte differentiation (Supp. Figure 6B). Furthermore, activation of the canonical
433 NF-κB pathway with TNFα inhibited adipocyte differentiation in WT C3H10T1/2 cells, whereas
434 preferential activation of the noncanonical NF-κB pathway with TWEAK did not inhibit
435 adipogenesis (Supp. Figure 6C,D).

436 Next, we observed that NIK and RelB were required for the induction of the essential
437 adipogenic transcription factors PPARγ and C/EBPα [40] (Figure 7C, Supp. Figure 6E). Ectopic
438 expression of NIK or RelB in NIK KO cells rescued their ability to respond to the PPARγ agonist
439 ETYA (eicosatetraynoic acid), and increased PPARγ and C/EBPα expression (Figure 7D, Supp.
440 Figure 6F). PPARγ was also observed to be decreased in NIK KO liver extracts (Supp. Figure
441 6G). Additionally, expression of the PPARγ-regulated, adipocyte-specific genes adiponectin
442 (*ADIPOQ*), glucose transporter 4 (GLUT4, *SLC2A4*), and glycerol-3-phosphate dehydrogenase
443 (*GPD1*), were significantly impaired in NIK KO and RelB KO cells, basally and in response to a
444 PPARγ agonist. Expression of PPARγ and adipogenic genes, as well as functional adipocyte
445 differentiation was restored in NIK KO cells by re-expression of NIK or RelB (Figure 7E).
446 Additionally, the overexpression of PPARγ or C/EBPα rescued adipocyte differentiation in NIK
447 KO C3H10T1/2 and 3T3-L1 cells, demonstrating that NIK KO cells fail to undergo adipogenesis
448 due to their inability to increase expression of these key adipogenic transcription factors (Figure
449 7F). Taken together, these findings indicate that NIK promotes adiposity through noncanonical
450 NF-κB/RelB-dependent regulation of PPARγ and C/EBPα expression.

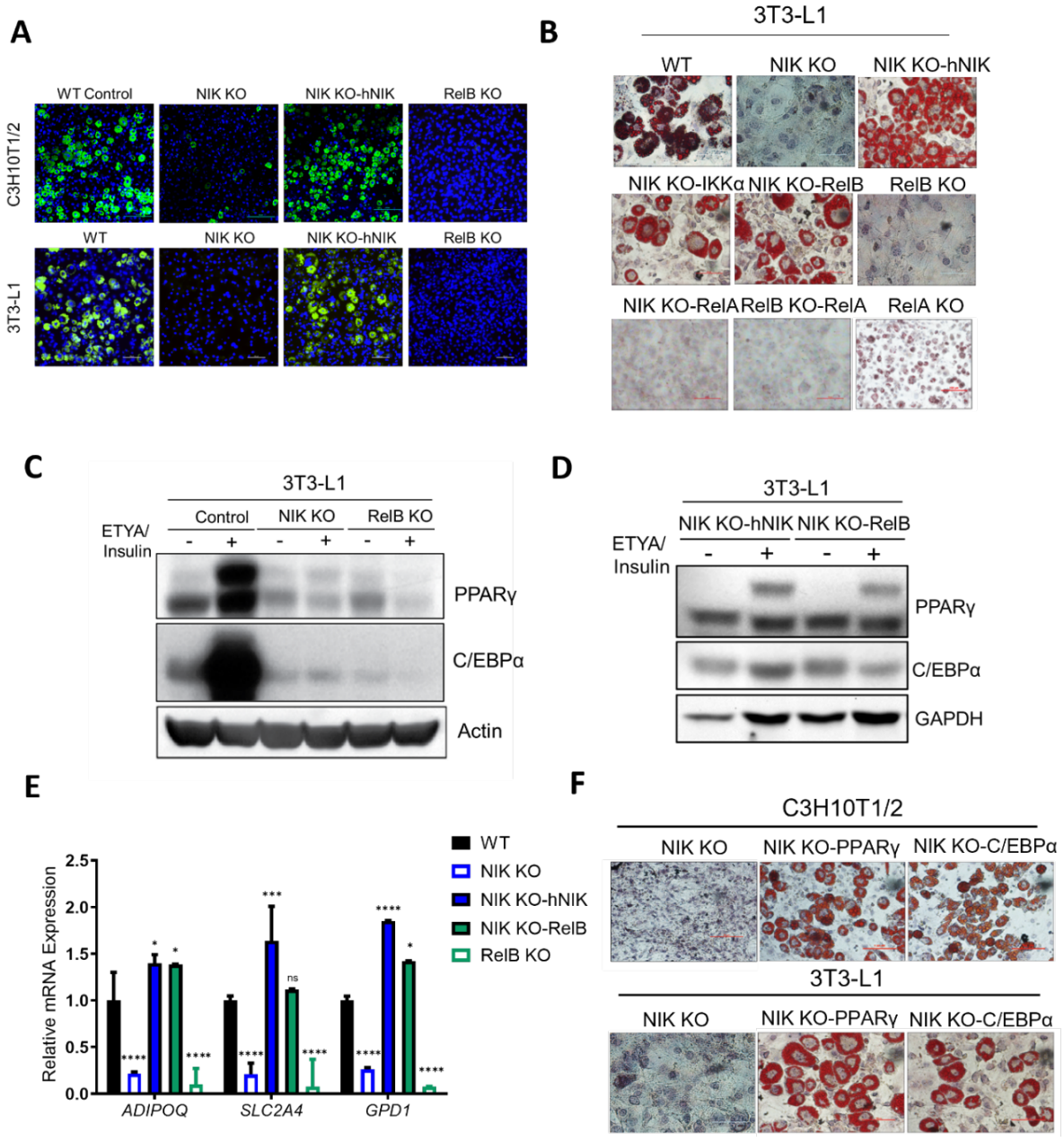

Figure 7: A role for noncanonical NF-κB-dependent signaling in promoting adiposity

(A) Fluorescent BODIPY lipid staining of C3H10T1/2 and 3T3-L1 cells showing a significant reduction in adipogenesis with the loss of NIK which is rescued in NIK KO-hNIK cells. **(B)** Oil Red O staining of differentiated 3T3-L1 cells lacking or over expressing various

457 noncanonical/canonical NF-κB proteins. **(C)** PPARγ and C/EBPα expression in undifferentiated
458 vs adipogenic treated in NIK KO and RelB KO 3T3-L1 cells compared to WT control cells. **(D)**
459 PPARγ and C/EBPα expression in undifferentiated vs adipogenic treated 3T3-L1 cells with re-
460 expression of human NIK or overexpression of RelB in NIK KO cells (NIK KO-hNIK, NIK KO-
461 RelB). **(E)** qPCR analysis of adipocyte genes (*ADIPOQ, SLC2A4, GPD1*) in ETYA/insulin treated
462 C3H10T1/2 cells. Data represented as mean ± SD, Tukey's Multiple Comparison Test. **(F)** Oil
463 Red O staining of differentiated NIK KO or NIK KO with overexpression of PPARγ or C/EBPα in
464 C3H10T1/2 and 3T3-L1 cells.

465

466 **3. Discussion**

467 Maintenance of energy balance is critical for normal physiological processes and overall
468 health status. In this study, we demonstrate that NIK is required to for metabolic homeostasis
469 through control of mitochondrial respiration and fitness, establishing a previously unrecognized
470 role for NIK in controlling cellular, tissue, and systemic metabolism in response to nutritional
471 stress. Consistent with *in vivo* findings, *in vitro* and *ex vivo* analysis revealed that NIK KO
472 preadipocytes and tissue exhibited impaired mitochondrial spare respiratory capacity and
473 elevated proton leak. Furthermore, we observed a compensatory upregulation of glycolysis in the
474 absence of NIK to meet energy demands (see Figs. 2, 3 & 6). This metabolic reprogramming has
475 parallels to the Warburg effect in cancer cells [41], which facilitates rapid generation of ATP using
476 glucose as a carbon source for anabolic pathways while controlling ROS production and redox
477 homeostasis [42]. Our results are also consistent with the use of glucose and glycolysis to reduce
478 ATP input for substrate catabolism, especially in a stressed state [29–31].

479 A key finding of our study is our observation that NIK-deficient exhibit higher energy
480 expenditure resulting in decreased adiposity, even under the chronic stress of overnutrition
481 caused by a HFD, which has been shown to induce oxidative stress and promote mitochondrial

482 dysfunction. We note that NIK KO mice were housed similarly to other immunodeficient animals
483 and analyzed at 2-4 months of age when they appeared healthy and exhibited no sign of infection
484 or dermatitis (see Figure 5A). Our data are consistent with a previous report demonstrating that
485 NIK activity is increased in the livers of genetic (*ob/ob)* or HFD-fed obese mice, and liver-specific
486 loss of NIK increases glucose metabolism [16,17]. Similarly, another group demonstrated that
487 NIK overexpression in pancreatic islet cells decreases insulin secretion and glucose homeostasis
488 [43], consistent with the increased glucose and insulin tolerance found in our NIK KO mice. In this
489 study, we analyzed adipose tissue as a key metabolic tissue that impacts local and systemic
490 metabolism. While male and female NIK KO mice exhibited reduced adiposity and elevated
491 metabolic demand, only females exhibited systemic metabolic changes under a chow-fed diet,
492 including increased energy expenditure and temperature. Elevated thermogenesis is consistent
493 with increased mitochondrial proton uncoupling due to higher proton leak observed in NIK KO
494 cells, as well as the increased brown adipose deposition in NIK KO mice (see Fig 4). Notably,
495 when challenged with a HFD, both genders exhibited a significant increase in energy expenditure
496 and higher glucose oxidation than WT mice, demonstrating that with overnutrition, glycolytic
497 adaptation is fueled to support the increase in energetic demand. Dimorphic sex differences in
498 energy expenditure might be attributed to distinct hormone-dependent metabolic or immune
499 changes between males and females. For example, although females are more prone to adipose
500 deposition than males, estrogen increases insulin sensitivity thereby protecting female mice from
501 diet-induced obesity [44–46], and estrogen also enhances mitochondrial function in adipocytes
502 [47]. Furthermore, a recent study demonstrated that RANKL/NIK signaling induced
503 postmenopausal obesity in ovariectomized $Nik^{aly/aly}$ mice, which exhibited reduced adipocyte
504 hypertrophy and reduced lipid accumulation, consistent with our findings that NIK promotes
505 adiposity and adipose development [48].

506 Interestingly, our findings revealed that NIK regulates adiposity through both NF-κB-
507 independent and NF-κB-dependent mechanisms. Notably, NIK regulates mitochondrial dynamics

508 and metabolism independently of downstream NF-κB RelB (see Figure 2). However, it promotes
509 adipocyte differentiation in noncanonical NF-κB-dependent manner, whereas canonical NF-κB
510 activity suppresses adipogenesis (see Figure 7). These observations are consistent with previous
511 data showing that activation or overexpression of the canonical NF-κB/RelA pathway inhibits
512 adipogenesis, and that RelA itself is inhibited by adipogenic-promoting PPARγ agonists *in vitro*
513 and *in vivo* [49,50]. Furthermore, one study demonstrated an increase of RelB and p52 during
514 adipocyte differentiation [51], while a separate study demonstrated that mice with adipose-specific
515 knockout of Tank-binding kinase 1 (TBK1), a repressor of NIK stability, exhibited a reduction in
516 adipose tissue and adipocyte size under a prolonged HFD [52]. However, a cooperative role for
517 the canonical and noncanonical NF-κB pathways in promoting adipocyte differentiation was
518 previously reported in a study of adipose-specific RelB knockout mice in response to lymphotoxin-
519 β-receptor (LTβR) activation [53]. Our results suggest that there are likely signal-specific roles for
520 RelB in regulating PPARγ expression and adipogenesis. Moreover, NIK may have RelB-
521 independent, or non-cell autonomous effects on adipogenesis and adipose development. In the
522 context of these findings, the signals responsible for activating NIK during adipocyte development
523 and expansion under a HFD warrant further study.

524 Further investigation is needed to understand if NIK has adipose cell-intrinsic effects *in*
525 *vivo*, as well as assess how other tissue types, such as skeletal muscle which is a major glucose
526 sink [54], regulate metabolic homeostasis *in vivo*. For example, NIK may impact systemic
527 metabolism indirectly through its regulation of immune functions, as changes in bacterial flora or
528 viral infection, which activate NIK/NF-κB signaling, can alter host metabolism to support
529 replication [55,56]. Furthermore, as a regulator of lymphoid development, NIK deficiency might
530 affect the metabolic status and recruitment of adipose tissue immune cells that can play critical
531 roles in regulating tissue homeostasis [14,57]. We note that *in vitro* preadipocytes exhibited
532 metabolic phenotypes similar to *ex vivo* adipose tissue (see Figs. 2 & 3), demonstrating that NIK
533 has similar adipocyte cell-intrinsic and tissue-specific metabolic functions.

534 Our analysis of NIK knockout mice provides new insight into the role of metabolic
535 dysfunction in the profoundly debilitating phenotypes of primary immunodeficiency diseases
536 (PIDs). Several genetic defects in the NF-κB signaling pathway are associated with PIDs [58–62],
537 including recently described patients with loss-of-function mutations in NIK [10,11]. Patients with
538 PIDs have been observed to have growth defects, mainly in children [63,64]. Risk for infection
539 have also been linked to factors including body mass index and adipose deposition due to the
540 immunomodulatory effects of the tissue, but less is understood of the metabolic dynamics in
541 patients with PIDs [65,66]. An intimate association between primary immunodeficiencies and
542 primary metabolic diseases is supported by the observation that mitochondrial disease patients
543 manifest significant immunological defects, [67,68], and some studies have linked inborn errors
544 of metabolism (IEM) as mimicking or exacerbating immune defects [69]. Overall, our findings are
545 consistent with the increasing appreciation that mitochondrial functions are important for
546 integrating metabolic cues and maintaining systemic metabolic health. Moreover, our work
547 highlights an important role for NIK in regulating metabolic homeostatic and adaptive adipose
548 remodeling mechanisms in response to a variety of disease contexts, including chronic stress due
549 to aging, immunodeficiency or overnutrition.

550

551 **Author Contributions:** Conceptualization: K.M.P., D.W.L., R.S.; Data Acquisition: K.M.P.,
552 D.W.L., J.K.; Writing—original draft preparation, K.M.P.; Writing—review and editing, K.M.P. and
553 R.S.; Visualization: K.M.P., R.S.; Funding acquisition: R.S.; Supervision: R.S. All authors have
554 read and agreed to the publication of the manuscript.

555

556 **Funding:** NIH-1R01NS082554 to R.S.

557 **Acknowledgments:** We thank Dr. Joseph M. Rutkowski for 3T3-L1 cells, Dr. Larry Suva and Dr.
558 Kirby for assistance with DEXA imaging, Dr. David Threadgill and his lab, including Dr. Alexandra
559 Trott and Orion Hicks at the Texas A&M Rodent Preclinical Phenotyping Core, for assistance with
560 the EchoMRI™ machine and TSE Phenomaster™ metabolic cages, and Texas A&M Health
561 Science Center COM-CAF core for use of the Seahorse machine.

562

563 **Conflicts of Interest:** The authors declare no conflicts of interest.

564

565

566 **4. Materials and Methods**

567

568 **4.1 Animal Procedures & *Ex Vivo* Work**

569 All animal experiments were done in accordance with animal use protocol (2019-0102) with
570 approved IACUC guidelines. *Map3k14* mice were purchased from Jackson lab (B6N.129-
571 Map3k14tm1Rds/J) and maintained by heterozygous breeding. Mice are housed on
572 hypoallergenic, alpha dry bedding with weekly cage changes to minimize dermatitis. Chow diet
573 contained 4% fat while HFD contained 45% fat (Lab Supply 58125). Mice analyzed on a HFD
574 were weaned from adult females on a HFD and then maintained on a HFD for at least 2 months.

575

576 **4.2 Cell Culture**

577 Mesenchymal stem cell line and preadipocyte cell line, C3H10T1/2 and 3T3-L1 were cultured in
578 DMEM supplemented with 10% FBS, 100 U/ml penicillin and 0.1mg/ml streptomycin (Thermo
579 Fisher Scientific, Waltham, MA). 293-T cells were obtained from ATCC (www.atcc.org) and
580 cultured in DMEM supplemented with 10% FBS, 100 U/ml penicillin and 0.1mg/ml streptomycin.

581 Bone marrow MSC cells were isolated from the femurs of mouse and cultured in DMEM
582 supplemented with 10% FBS, 100 U/ml penicillin and 0.1mg/ml streptomycin.
583
584 **4.3 Bone Marrow Cell Isolation**
585 Mouse femurs are collected and sterilized in 70% ethanol and then were crushed in sterile PBS
586 in a mortar with a pestle. From the crushed femurs, 5mL of DMEM (with 10% FBS and 1%
587 penicillin/streptomycin) is then used to collected cells into a conical tube through a 70μM filter.
588 Cells are then centrifuged at 1500rpm for 8 minutes. Media is removed and the cell pellet is
589 resuspended in 3mL of ACK lysis buffer (Lonza 10-548E) for 2 minutes. ACK cell suspension is
590 diluted with 10mL of media and pelleted again. The cell pellet is resuspended in 10mL of media
591 and filtered through a 40μM filter.
592
593 **4.4 CRISPR-Cas9 Gene Knockout**
594 Oligos encoding guide RNAs for murine NIK and RelB are found in Supplemental Table 1. Each
595 gRNAs were cloned into Lenti-CrispR-v2 (Addgene, Cambridge, MA) respectively. C3H10T1/2
596 and 3T3-L1 cells were transduced with a mixture of lentiviruses (described below) carrying the
597 three murine gRNAs. Puromycin resistant single clonal cells were isolated by serial dilution and
598 experiments were repeated with at least two clones. Loss of NIK or RelB expression was
599 confirmed by immunoblot analysis. For controls, cells were transduced with empty LentiCrispR-
600 V2.
601
602 **4.5 Lentivirus Production**
603 Lentiviral construct of over-expression constructs (NIK, IKKα, RelB, RelA, PPARγ and C/EBPα)
604 was obtained from DNASU (Tempe, AZ). 24μg of lentiviral plasmids and 72μg of
605 polyethyleneimine (Sigma-Aldrich) were used to transfect 293T cells. After 3 days of transfection,
606 viral supernatant was concentrated 20 fold, to 500μl using Lenti-X Concentrator (Clontech,

607 Mountain View, CA), and 100µl of concentrated virus was used to infect cells. Stably transduced
608 cells were selected for 72hr in medium containing 0.6µg/ml puromycin or 6µg/ml blasticidin
609 (Thermo Fisher).
610
611 **4.6 Seahorse Extracellular Flux Analysis**
612 **4.6.1 3T3-L1 Cells**
613 Metabolic activity was analyzed using a Seahorse XFe96 Analyzer (Agilent, Santa Clara, CA).
614 For 3T3-L1 cells, forty-thousand cells per well were plated in the collagen-coated (40ng/µL)
615 Agilent Seahorse XFe96 microplates day before analysis. Mitochondrial Stress Tests were
616 conducted according to the manufacturer's guidelines. Base media was supplemented with 25mM
617 glucose (Sigma, G7021, St. Louis, MO), 2mM glutamine (Sigma, G85420, St. Louis, MO), and
618 1mM pyruvate (Gibco). Inhibitors were used at the following final concentrations (10x inhibitor
619 was added to injection ports to reach final concentration): 1µM oligomycin A (Sigma, 75351, St.
620 Louis, MO), 2µM FCCP (Sigma, C2920, St. Louis, MO), and mixture of 0.5µM rotenone (Enzo
621 Life Sciences, Farmingdale, NY, ALX-350-360) and 0.5µM antimycin A (Sigma, A8674, St. Louis,
622 MO). For Glycolysis Stress Tests, cells were glucose-starved for 1hr in Seahorse DMEM base
623 media with 2mM glutamine before analysis. Reagents for injections were used at the following
624 final concentrations (10x reagent was added to injection ports to reach final concentration): 10mM
625 glucose, 10uM oligomycin A, 50mM 2-DG (Thermo Fischer Scientific, 50-519-066). After
626 Seahorse analysis, DNA content was measured using DRAQ5 staining (Thermo Fisher Scientific,
627 50-712-282) for normalization. Assay was ran in 3 biological replicates with samples ran in 5-8
628 replicates per assay. Analyses were conducted using Seahorse Wave Controller Software v2.6
629 and XF Report Generators (Agilent Technologies).
630
631 **4.6.2 *Ex Vivo* Adipose Tissue**

632 Analysis of metabolic activity of adipose tissue was adapted from [70]. 96 well Seahorse plates
633 were coated twice with Cell-Tak (50µg/mL, Corning® Cell-Tak™ Cell and Tissue Adhesive, Cat.
634 No. 354240). Tissue was excised fresh, rinsed well in PBS, and cut into small, >1mg, pieces of
635 similar size and plated into the center of the wells. For Mitochondria Stress Test, base media was
636 supplemented with 25 mM glucose, 2 mM glutamine, and 1 mM pyruvate. Inhibitors were used at
637 the following final concentrations (10x inhibitor was added to injection ports to reach final
638 concentration): 20µM oligomycin A, 20µM FCCP, and mixture of 20µM rotenone and 20µM
639 antimycin A. Tissue samples are ran in 5-10 replicates per tissue type per assay. Seahorse
640 Analyses were done following Agilent guidelines for the mitochondria stress test [71] and energy
641 phenotyping [72].
642 For Glycolysis Stress Test base media was supplemented with 2mM glutamine, and reagents for
643 injections were used at the following final concentrations (10x reagent was added to injection
644 ports to reach final concentration): 25mM glucose, 20µM oligomycin A, 100mM 2-DG. Run time
645 for tissue was increased to 30 minutes per injection with four measurements per compound (4
646 cycles of 3 min mix, 1.5 min wait, 3 min measure). Analyses of glycolysis stress test was done
647 following Agilent guidelines [73]. Afterwards, tissue was homogenized, lysed, and normalized by
648 protein.
649
650 **4.7 Immunofluorescence**
651 For immunofluorescence of C3H10T1/2 mitochondria staining, cells were transfected with 1µg
652 DsRed2-Mito-7 (Mito-dsRed) (Addgene Plasmid #55838) by lipofectamine (Invitrogen L3000008)
653 for 48-72hrs or stained with COXIV 1:200 overnight. Cells were then fixed with 4% PFA for 20
654 minutes at 37°C. After fixation, cells were washed with PBS and then stained with a fluorescent
655 secondary and/or Hoechst (1:1000) diluted in 1% BSA, .1% Triton-X in PBS. Cells were imaged
656 by confocal (Nikon TI A1R inverted confocal microscope).
657

658 **4.8 BODIPY Staining**

659 For immunofluorescence imaging, BODIPY™ 490/509 (4,4-Difluoro-1,3,5,7,8-Pentamethyl-4-
660 Bora-3a,4a-Diaza-s-Indacene) (Sigma Aldrich 790389) was used. 5mM of BODIPY dye was
661 diluted 1:2500 in PBS and incubate on live cells for 10 minutes at 37°C. Afterwards, cells were
662 washed twice with PBS and then fixed in 4% PFA for 20 minutes at 37°C. After fixation, cells were
663 washed twice with PBS and then stained with Hoechst (1:1000) diluted in 1% BSA, .1% Triton-X
664 in PBS for 10 minutes. Cells were imaged by confocal (Nikon TI A1R inverted confocal
665 microscope).

666

667 **4.9 Lipolysis**

668 About 2-5mg was placed in a 12 well plate in duplicate or triplicate. Tissue was left to sit in 300μL
669 DMEM without FBS for an hour in the incubator. Media was removed for t=0 and isoproterenol
670 was added for a final concentration of 100μM. Tissue was incubated with the isoproterenol for an
671 hour and then media was removed for t=1 timepoint, final samples were taken after overnight
672 incubation. 10μL of each sample at the different points were mixed with 160μL of glycerol reagent
673 (Sigma, F6428) and read at an absorbance of 540nm for glycerol levels.

674

675 **4.10 Adipocyte Differentiation**

676 Adipocyte differentiation was induced by treating confluent cells for 2 days with 5 mg/ml insulin
677 (Thermo Fisher Scientific) and 10μM ETYA (Santa Cruz Biotech, Dallas, TX) in Dulbecco's
678 modified Eagle's medium containing 10% FBS, and then every 2 days for 6 Days with insulin (5
679 mg./ml). Treatment with NIK inhibitor B022 was purchased from MEDCHEM EXPRESS (Cat. No.
680 HY-120501) and used at a concentration of 5μM, TNFα (ProSpec CYT-223) and TWEAK
681 (PeproTech 31006) were used at 10ng/mL.

682

683 **4.11 Oil Red O Staining**

684 For the Oil Red O staining, Oil Red O staining solution (0.5% Oil-Red O in isopropyl alcohol
685 solution-distilled water [60:40]) was filtered through the Whatman no. 1 filter paper. Cells were
686 fixed with 10% formaldehyde solution for 30 min at 37°C, then washed with 60% isopropyl alcohol
687 followed by staining with the filtered Oil Red O solution for 20 min and then washed with distilled
688 water three times. To measure Oil Red O staining of adipocyte differentiated cells, dye is eluted
689 with 100% isopropanol for 10 minutes. Eluted dye is transferred to 96 well plate and optical density
690 measurements were done on Perkin Elmer plate reader at 500nm, .5 sec.
691
692 **4.12 Immunoblot**
693 Cells were lysed in RIPA lysis buffer (Thermo Fisher Scientific) with protease/phosphatase
694 inhibitor cocktail (Thermo Fisher Scientific). Protein was mixed with NuPage 4X LDS sample
695 buffer (Thermo Fisher Scientific) containing .1M DTT and denatured at 100˚C for 7 min. Proteins
696 were separated on 8% ~ 12% SDS-PAGE and transferred to nitrocellulose membranes
697 (Amersham). The membranes were blocked for 1h with 5% non-fat dry milk in 0.1% Tween-
698 20/TBS (TBST) and incubated with primary antibodies diluted in blocking buffer at 4°C overnight.
699 After washing in TBST, membranes were incubated with secondary in BSA for 1 hour at room
700 temperature. The blots were washed with TBST and developed using Chemiluminescent HRP
701 Substrate (EMD Millipore) on ChemiDoc MP Imaging System (Bio-Rad) for detection of HRP or
702 an Odyssey Infrared Imaging system (LI-COR Biosciences) for detection of IRDye fluorescent
703 dyes.
704
705 **4.13 Antibodies**
706 Following antibodies were used C/EBPα (CST8178) (Cell Signaling Technology), COXIV
707 (CST11967s), GPD1 (sc-376219) (Santa Cruz Biotechnology, Dallas, TX), IKKα (CST2682),
708 NFKB2 (CST4882), NIK (CST4994), p-RelA (p-p65) (CST3033), RelA (p65) (sc-8008), PPARγ
709 (CST2443), RelB (CST4992), GAPDH (sc137179), and β-actin (sc69879).

710

711 **4.14 RNA Isolation, cDNA Synthesis, and Quantitative-RT-PCR**

712 Primers used for qPCR are in Supplemental Table 2.

713 **4.14.1 Cells:** Total RNA was isolated from cells by Purelink™ RNA Mini Kit (Life Technologies).
714 cDNA was synthesized from 1 µg total RNA using iScript reverse transcription supermix (Bio-Rad,
715 Hercules, CA) following the manufacturer's protocol. Quantitative RT-PCR was performed using
716 iTaq Universal SYBR Green Supermix (Bio-Rad) with StepOnePlus Real-Time PCR System
717 (Applied Biosystems, Foster City, CA).

718 **4.14.2 Tissue:** Mouse tissue was frozen with liquid nitrogen and ground to a powder with a pestle
719 in a mortar (a minimum of 50mg of tissue is needed, for WAT 1g may be needed). Tissue was
720 then lysed with Trizol (1mL per gram of tissue), followed by addition of chloroform to centrifuged
721 supernatant (200µL chloroform: 1mL Trizol). Equal amounts of 70% ethanol was added to equal
722 parts of aqueous layer from sample in a new tube and then RNA was then collected in subsequent
723 steps using Invitrogen Purelink RNA mini kit. Zymo DNAse was used with 40-80µL per sample.
724 cDNA was synthesized from 2µg of RNA using iScript reverse transcriptase and buffer mix.
725 Samples were ran in triplicate.

726

727 **4.15 EchoMRI™**

728 EchoMRI™ 100H machine was used to analyze fat and lean mass of chow and HFD mice at 2 or
729 4 months of age. Mice were weighed before imaging and imaged in MRI tubes.

730

731 **4.16 DEXA Imaging**

732 Dual-energy x-ray absorptiometry was used on anesthetize mice to visualize low and high-density
733 tissue. Mice from maintained on either a chow or HFD were used.

734

735 **4.17 Metabolic Cages**

736 Metabolic analysis on the mice was conducted in TSE Phenomaster™ metabolic cages through
737 Rodent Preclinical Phenotyping Core at TAMU (https://genomics.tamu.edu/preclinical-
738 phenotyping/). Mice were weighed the day of and housed individually for 48hrs. Data was
739 analyzed based on last 24hrs to compensate for mouse adjustment to the new environment.
740

741 **4.18 Glucose Tolerance Testing**

742 For glucose tolerance testing mice were morning fasted for 6hrs in clean cages. Mice were
743 weighed, and from tail clip, initial glucose levels are recorded using a glucose meter. The mice
744 are then intraperitoneally injected with 20% D-glucose at 2g/kg (μL= 10 x BW). Blood glucose (in
745 mg/dL) is then recorded at t=15, t=30, t=60, t=120 minutes post injection.
746

747 **4.19 Insulin Tolerance Testing**

748 For insulin tolerance testing mice were morning fasted for 4hrs in clean cages. Mice were weighed
749 and from tail clip initial glucose levels are recorded using a glucose meter. The mice are then
750 intraperitoneally injected with .5 U/kg Insulin (μL= 5 x BW of .1 U/mL insulin). Blood glucose (in
751 mg/dL) is then recorded at t=15, t=30, t=45, t=60, t=90 minutes post injection.
752

753 **4.20 Statistical Analysis**

754 Statistical Analysis was done using GraphPad PRISM software, specifics on data representation
755 and tests used for analysis can be found in figure legends. *p ≤.05, ** p ≤.01, *** p ≤.001, ****
756 p≤.0001. Unpaired student t-tests were ran as two-tailed. All statistically significant analyses were
757 ran based on a 95% confidence interval.

758

759

760 **References**

761 [1] Yin, L., Wu, L., Wesche, H., Arthur, C.D., White, J.M., Goeddel, D.V., et al., 2001. Defective
762 lymphotoxin-beta receptor-induced NF-kappaB transcriptional activity in NIK-deficient mice.
763 Science (New York, N.Y.) 291(5511): 2162–5, Doi: 10.1126/science.1058453.
764 [2] Xiao, G., Fong, A., Sun, S.C., 2004. Induction of p100 processing by NF-kappaB-inducing kinase
765 involves docking IkappaB kinase alpha (IKKalpha) to p100 and IKKalpha-mediated phosphorylation.
766 J Biol Chem 279(29): 30099–105.
767 [3] Akemi Matsushima, T.K., 2001. Essential role of nuclear factor (NF)-κB-inducing kinase and
768 inhibitor of κB (IκB) kinase α in NF-κB activation through lymphotoxin β receptor, but not through
769 tumor necrosis factor receptor I. Journal of Experimental Medicine 193: 631–6.
770 [4] Sun, S.C., 2011. Non-canonical NF-kappaB signaling pathway. Cell Res 21(1): 71–85.
771 [5] Shinkura, R., Kitada, K., Matsuda, F., Tashiro, K., Ikuta, K., Suzuki, M., et al., 1999. Alymphoplasia is
772 caused by a point mutation in the mouse gene encoding Nf-κb-inducing kinase. Nature Genetics
773 22(1): 74–7, Doi: 10.1038/8780.
774 [6] Brightbill, H.D., Jackman, J.K., Suto, E., Kennedy, H., Jones, C., Chalasani, S., et al., 2015. Conditional
775 Deletion of NF-kappaB-Inducing Kinase (NIK) in Adult Mice Disrupts Mature B Cell Survival and
776 Activation. J Immunol 195(3): 953–64.
777 [7] Li, Y., Wang, H., Zhou, X., Xie, X., Chen, X., Jie, Z., et al., 2016. Cell intrinsic role of NF-kappaB-
778 inducing kinase in regulating T cell-mediated immune and autoimmune responses. Sci Rep 6:
779 22115.
780 [8] Lacher, S.M., Thurm, C., Distler, U., Mohebiany, A.N., Israel, N., Kitic, M., et al., 2018. NF-kappaB
781 inducing kinase (NIK) is an essential post-transcriptional regulator of T-cell activation affecting F-
782 actin dynamics and TCR signaling. J Autoimmun 94: 110–21.
783 [9] Hamdan, T.A., Bhat, H., Cham, L.B., Adomati, T., Lang, J., Li, F., et al., 2020. Map3k14 as a Regulator
784 of Innate and Adaptive Immune Response during Acute Viral Infection. Pathogens (Basel,
785 Switzerland) 9(2), Doi: 10.3390/pathogens9020096.
786 [10] Willmann, K.L., Klaver, S., Dogu, F., Santos-Valente, E., Garncarz, W., Bilic, I., et al., 2014. Biallelic
787 loss-of-function mutation in NIK causes a primary immunodeficiency with multifaceted aberrant
788 lymphoid immunity. Nat Commun 5: 5360.
789 [11] Schlechter, N., Glanzmann, B., Hoal, E.G., Schoeman, M., Petersen, B.S., Franke, A., et al., 2017.
790 Exome Sequencing Identifies a Novel MAP3K14 Mutation in Recessive Atypical Combined
791 Immunodeficiency. Front Immunol 8: 1624.
792 [12] Gu, M., Zhou, X., Sohn, J.H., Zhu, L., Jie, Z., Yang, J.-Y., et al., 2021. NF-κB-inducing kinase maintains
793 T cell metabolic fitness in antitumor immunity. Nature Immunology 22(2): 193–204, Doi:
794 10.1038/s41590-020-00829-6.
795 [13] Jung, J.U., Ravi, S., Lee, D.W., McFadden, K., Kamradt, M.L., Toussaint, L.G., et al., 2016.
796 NIK/MAP3K14 Regulates Mitochondrial Dynamics and Trafficking to Promote Cell Invasion. Curr
797 Biol 26(24): 3288–302.
798 [14] Keeney, J.N., Winters, A., Sitcheran, R., West, A.P., 2022. NF-κB-Inducing Kinase (NIK) Governs the
799 Mitochondrial Respiratory Capacity, Differentiation, and Inflammatory Status of Innate Immune
800 Cells. Immunology.
801 [15] Kamradt, M.L., Jung, J.-U., Pflug, K.M., Lee, D.W., Fanniel, V., Sitcheran, R., 2021. NIK promotes
802 metabolic adaptation of glioblastoma cells to bioenergetic stress. Cell Death & Disease 12(3): 1–18,
803 Doi: 10.1038/s41419-020-03383-z.

[16] Sheng, L., Zhou, Y., Chen, Z., Ren, D., Cho, K.W., Jiang, L., et al., 2012. NF-kappaB-inducing kinase (NIK) promotes hyperglycemia and glucose intolerance in obesity by augmenting glucagon action. Nat Med 18(6): 943–9.

[17] Liu, Y., Sheng, L., Xiong, Y., Shen, H., Liu, Y., Rui, L., 2017. Liver NF-kappaB-Inducing Kinase Promotes Liver Steatosis and Glucose Counterregulation in Male Mice With Obesity. Endocrinology 158(5): 1207–16.

[18] Li, Y., Chen, M., Zhou, Y., Tang, C., Zhang, W., Zhong, Y., et al., 2020. NIK links inflammation to hepatic steatosis by suppressing PPARalpha in alcoholic liver disease. Theranostics 10(8): 3579–93.

[19] Pang, G., Xie, J., Chen, Q., Hu, Z., 2014. Energy intake, metabolic homeostasis, and human health. Food Science and Human Wellness 3(3): 89–103, Doi: 10.1016/j.fshw.2015.01.001.

[20] O'Brien, C.M., Mulukutla, B.C., Mashek, D.G., Hu, W.-S., 2020. Regulation of Metabolic Homeostasis in Cell Culture Bioprocesses. Trends in Biotechnology 38(10): 1113–27, Doi: 10.1016/j.tibtech.2020.02.005.

[21] Ma, Y., Li, J., 2015. Metabolic Shifts during Aging and Pathology. Comprehensive Physiology 5(2): 667–86, Doi: 10.1002/cphy.c140041.

[22] Picard, M., McEwen, B.S., Epel, E.S., Sandi, C., 2018. An energetic view of stress: Focus on mitochondria. Frontiers in Neuroendocrinology 49: 72–85, Doi: 10.1016/j.yfrne.2018.01.001.

[23] Li, Y., Jia, A., Wang, Y., Dong, L., Wang, Y., He, Y., et al., 2019. Immune effects of glycolysis or oxidative phosphorylation metabolic pathway in protecting against bacterial infection. Journal of Cellular Physiology 234(11): 20298–309, Doi: https://doi.org/10.1002/jcp.28630.

[24] Yuan, X., Liu, Y., Bijonowski, B.M., Tsai, A.-C., Fu, Q., Logan, T.M., et al., 2020. NAD + /NADH redox alterations reconfigure metabolism and rejuvenate senescent human mesenchymal stem cells in vitro. Communications Biology 3(1): 1–15, Doi: 10.1038/s42003-020-01514-y.

[25] Duan, K., Liu, Z.-J., Hu, S.-Q., Huo, H.-Y., Xu, Z.-R., Ruan, J.-F., et al., 2018. Lactic acid induces lactate transport and glycolysis/OXPHOS interconversion in glioblastoma. Biochemical and Biophysical Research Communications 503(2): 888–94, Doi: 10.1016/j.bbrc.2018.06.092.

[26] Bar-Even, A., Flamholz, A., Noor, E., Milo, R., 2012. Rethinking glycolysis: on the biochemical logic of metabolic pathways. Nature Chemical Biology 8(6): 509–17, Doi: 10.1038/nchembio.971.

[27] Rodic, S., Vincent, M.D., 2018. Reactive oxygen species (ROS) are a key determinant of cancer's metabolic phenotype. International Journal of Cancer 142(3): 440–8, Doi: https://doi.org/10.1002/ijc.31069.

[28] Li, X., Jiang, Y., Meisenhelder, J., Yang, W., Hawke, D.H., Zheng, Y., et al., 2016. Mitochondria-Translocated PGK1 Functions as a Protein Kinase to Coordinate Glycolysis and the TCA Cycle in Tumorigenesis. Molecular Cell 61(5): 705–19, Doi: 10.1016/j.molcel.2016.02.009.

[29] Even, P.C., Nadkarni, N.A., 2012. Indirect calorimetry in laboratory mice and rats: principles, practical considerations, interpretation and perspectives. American Journal of Physiology-Regulatory, Integrative and Comparative Physiology 303(5): R459–76, Doi: 10.1152/ajpregu.00137.2012.

[30] Mizock, B.A., 1995. Alterations in carbohydrate metabolism during stress: A review of the literature. The American Journal of Medicine 98(1): 75–84, Doi: 10.1016/S0002-9343(99)80083-7.

[31] Livesey, G., Elia, M., 1988. Estimation of energy expenditure, net carbohydrate utilization, and net fat oxidation and synthesis by indirect calorimetry: evaluation of errors with special reference to the detailed composition of fuels. The American Journal of Clinical Nutrition 47(4): 608–28, Doi: 10.1093/ajcn/47.4.608.

[32] Marchetti, P., Fovez, Q., Germain, N., Khamari, R., Kluza, J., 2020. Mitochondrial spare respiratory capacity: Mechanisms, regulation, and significance in non-transformed and cancer cells. The FASEB Journal 34(10): 13106–24, Doi: https://doi.org/10.1096/fj.202000767R.

851 [33] Sriskanthadevan, S., Jeyaraju, D.V., Chung, T.E., Prabha, S., Xu, W., Skrtic, M., et al., 2015. AML cells
852 have low spare reserve capacity in their respiratory chain that renders them susceptible to
853 oxidative metabolic stress. Blood 125(13): 2120–30, Doi: 10.1182/blood-2014-08-594408.
854 [34] van der Windt, G.J.W., Everts, B., Chang, C.-H., Curtis, J.D., Freitas, T.C., Amiel, E., et al., 2012.
855 Mitochondrial Respiratory Capacity Is a Critical Regulator of CD8+ T Cell Memory Development.
856 Immunity 36(1): 68–78, Doi: 10.1016/j.immuni.2011.12.007.
857 [35] Haas, R.H., Parikh, S., Falk, M.J., Saneto, R.P., Wolf, N.I., Darin, N., et al., 2007. Mitochondrial
858 disease: a practical approach for primary care physicians. Pediatrics 120(6): 1326–33, Doi:
859 10.1542/peds.2007-0391.
860 [36] Parikh, S., Goldstein, A., Koenig, M.K., Scaglia, F., Enns, G.M., Saneto, R., et al., 2015. Diagnosis and
861 management of mitochondrial disease: a consensus statement from the Mitochondrial Medicine
862 Society. Genetics in Medicine: Official Journal of the American College of Medical Genetics 17(9):
863 689–701, Doi: 10.1038/gim.2014.177.
864 [37] Mota, M., Banini, B.A., Cazanave, S.C., Sanyal, A.J., 2016. Molecular mechanisms of lipotoxicity and
865 glucotoxicity in nonalcoholic fatty liver disease. Metabolism 65(8): 1049–61.
866 [38] Pan, X., Wang, P., Luo, J., Wang, Z., Song, Y., Ye, J., et al., 2015. Adipogenic changes of hepatocytes
867 in a high-fat diet-induced fatty liver mice model and non-alcoholic fatty liver disease patients.
868 Endocrine 48(3): 834–47.
869 [39] Li, Z., Li, X., Su, M.B., Gao, L.X., Zhou, Y.B., Yuan, B., et al., 2020. Discovery of a Potent and Selective
870 NF-kappaB-Inducing Kinase (NIK) Inhibitor That Has Anti-inflammatory Effects in Vitro and in Vivo. J
871 Med Chem 63(8): 4388–407.
872 [40] Rosen, E.D., 2002. C/EBPalpha induces adipogenesis through PPARgamma : a unified pathway.
873 Genes & Development 16(1): 22–6, Doi: 10.1101/gad.948702.
874 [41] Calabrese, C., Iommarini, L., Kurelac, I., Calvaruso, M.A., Capristo, M., Lollini, P.-L., et al., 2013.
875 Respiratory complex I is essential to induce a Warburg profile in mitochondria-defective tumor
876 cells. Cancer & Metabolism 1(1): 11, Doi: 10.1186/2049-3002-1-11.
877 [42] Liberti, M.V., Locasale, J.W., 2016. The Warburg Effect: How Does it Benefit Cancer Cells? Trends in
878 Biochemical Sciences 41(3): 211–8, Doi: 10.1016/j.tibs.2015.12.001.
879 [43] Li, X., Jia, L., Chen, X., Dong, Y., Ren, X., Dong, Y., et al., 2018. Islet α-cell Inflammation Induced By
880 NF-κB inducing kinase (NIK) Leads to Hypoglycemia, Pancreatitis, Growth Retardation, and
881 Postnatal Death in Mice. Theranostics 8(21): 5960–71, Doi: 10.7150/thno.28960.
882 [44] Mauvais-Jarvis, F., 2015. Sex differences in metabolic homeostasis, diabetes, and obesity. Biology
883 of Sex Differences 6, Doi: 10.1186/s13293-015-0033-y.
884 [45] Riant, E., Waget, A., Cogo, H., Arnal, J.-F., Burcelin, R., Gourdy, P., 2009. Estrogens Protect against
885 High-Fat Diet-Induced Insulin Resistance and Glucose Intolerance in Mice. Endocrinology 150(5):
886 2109–17, Doi: 10.1210/en.2008-0971.
887 [46] Handgraaf, S., Riant, E., Fabre, A., Waget, A., Burcelin, R., Liere, P., et al., 2013. Prevention of
888 Obesity and Insulin Resistance by Estrogens Requires ER Activation Function-2 (ER AF-2), Whereas
889 ER AF-1 Is Dispensable. Diabetes 62(12): 4098–108, Doi: 10.2337/db13-0282.
890 [47] Bauzá-Thorbrügge, M., Rodríguez-Cuenca, S., Vidal-Puig, A., Galmés-Pascual, B.M., Sbert-Roig, M.,
891 Gianotti, M., et al., 2019. GPER and ERα mediate estradiol enhancement of mitochondrial function
892 in inflamed adipocytes through a PKA dependent mechanism. The Journal of Steroid Biochemistry
893 and Molecular Biology 185: 256–67, Doi: 10.1016/j.jsbmb.2018.09.013.
894 [48] Mori, K., Mizokami, A., Sano, T., Mukai, S., Hiura, F., Ayukawa, Y., et al., 2022. RANKL elevation
895 activates the NIK/NF-κB pathway, inducing obesity in ovariectomized mice. Journal of
896 Endocrinology 254(1): 27–36, Doi: 10.1530/JOE-21-0424.

[49] Tang, T., Zhang, J., Yin, J., Staszkiewicz, J., Gawronska-Kozak, B., Jung, D.Y., et al., 2010. Uncoupling of inflammation and insulin resistance by NF-kappaB in transgenic mice through elevated energy expenditure. J Biol Chem 285(7): 4637–44.

[50] Pascal Peraldi, M.X., 1997. Thiazolidinediones Block Tumor Necrosis Factor-a-induced Inhibition of insulin signaling. J. Clin. Invest. Volume 100(7): 1863–9.

[51] Berg, A.H., Lin, Y., Lisanti, M.P., Scherer, P.E., 2004. Adipocyte differentiation induces dynamic changes in NF-κB expression and activity. American Journal of Physiology-Endocrinology and Metabolism 287(6): E1178–88, Doi: 10.1152/ajpendo.00002.2004.

[52] Zhao, P., Wong, K. in., Sun, X., Reilly, S.M., Uhm, M., Liao, Z., et al., 2018. TBK1 at the Crossroads of Inflammation and Energy Homeostasis in Adipose Tissue. Cell 172(4): 731-743.e12, Doi: 10.1016/j.cell.2018.01.007.

[53] Weidemann, A., Lovas, A., Rauch, A., Andreas, N., von Maltzahn, J., Riemann, M., et al., 2016. Classical and alternative NF-kappaB signaling cooperate in regulating adipocyte differentiation and function. Int J Obes (Lond) 40(3): 452–9.

[54] Merz, K.E., Thurmond, D.C., 2020. Role of Skeletal Muscle in Insulin Resistance and Glucose Uptake. Comprehensive Physiology, John Wiley & Sons, Ltd p. 785–809.

[55] Eisenreich, W., Rudel, T., Heesemann, J., Goebel, W., 2019. How Viral and Intracellular Bacterial Pathogens Reprogram the Metabolism of Host Cells to Allow Their Intracellular Replication. Frontiers in Cellular and Infection Microbiology 9, Doi: 10.3389/fcimb.2019.00042.

[56] Sanchez, E.L., Lagunoff, M., 2015. Viral activation of cellular metabolism. Virology 479–480: 609–18, Doi: 10.1016/j.virol.2015.02.038.

[57] DeFuria, J., Belkina, A.C., Jagannathan-Bogdan, M., Snyder-Cappione, J., Carr, J.D., Nersesova, Y.R., et al., 2013. B cells promote inflammation in obesity and type 2 diabetes through regulation of T-cell function and an inflammatory cytokine profile. Proceedings of the National Academy of Sciences of the United States of America 110(13): 5133–8, Doi: 10.1073/pnas.1215840110.

[58] Smith, T., Cunningham-Rundles, C., 2019. Primary B-Cell Immunodeficiencies. Human Immunology 80(6): 351–62, Doi: 10.1016/j.humimm.2018.10.015.

[59] Wang, H.-Y., Ma, C.A., Zhao, Y., Fan, X., Zhou, Q., Edmonds, P., et al., 2013. Antibody deficiency associated with an inherited autosomal dominant mutation in TWEAK. Proceedings of the National Academy of Sciences of the United States of America 110(13): 5127–32, Doi: 10.1073/pnas.1221211110.

[60] Losi, C.G., Silini, A., Fiorini, C., Soresina, A., Meini, A., Ferrari, S., et al., 2005. Mutational analysis of human BAFF receptor TNFRSF13C (BAFF-R) in patients with common variable immunodeficiency. Journal of Clinical Immunology 25(5): 496–502, Doi: 10.1007/s10875-005-5637-2.

[61] Tuijnenburg, P., Lango Allen, H., Burns, S.O., Greene, D., Jansen, M.H., Staples, E., et al., 2018. Loss-of-function nuclear factor κB subunit 1 (NFKB1) variants are the most common monogenic cause of common variable immunodeficiency in Europeans. The Journal of Allergy and Clinical Immunology 142(4): 1285–96, Doi: 10.1016/j.jaci.2018.01.039.

[62] Chen, K., Coonrod, E.M., Kumánovics, A., Franks, Z.F., Durtschi, J.D., Margraf, R.L., et al., 2013. Germline mutations in NFKB2 implicate the noncanonical NF-κB pathway in the pathogenesis of common variable immunodeficiency. American Journal of Human Genetics 93(5): 812–24, Doi: 10.1016/j.ajhg.2013.09.009.

[63] Pieniawska-Śmiech, K., Bar, K., Babicki, M., Śmiech, K., Lewandowicz-Uszyńska, A., 2020. Assessment of weight and height of patients with primary immunodeficiency disorders and group of children with recurrent respiratory tract infections. BMC Immunology 21: 42, Doi: 10.1186/s12865-020-00372-x.

943 [64] Caetano, M.C., Silva, R., Ferreira, C.A., Sarni, R.O.S., Carvalho, B.T.C., 2011. Lipid Profile In Patients
944 With Primary Immunodeficiency. Journal of Allergy and Clinical Immunology 127(2, Supplement):
945 AB65, Doi: 10.1016/j.jaci.2010.12.269.
946 [65] Dobner, J., Kaser, S., 2018. Body mass index and the risk of infection - from underweight to
947 obesity. Clinical Microbiology and Infection 24(1): 24–8, Doi: 10.1016/j.cmi.2017.02.013.
948 [66] Ruffner, M.A., Sullivan, K.E., 2016. Body Weight and Infectious Outcomes in Patients with Primary
949 Immunodeficiency Diseases: Outcomes from within the US Immunodeficiency Network (USIDNET).
950 Journal of Allergy and Clinical Immunology 137(2): AB179, Doi: 10.1016/j.jaci.2015.12.718.
951 [67] Parikh, S., Goldstein, A., Karaa, A., Koenig, M.K., Anselm, I., Brunel-Guitton, C., et al., 2017. Patient
952 care standards for primary mitochondrial disease: a consensus statement from the Mitochondrial
953 Medicine Society. Genetics in Medicine: Official Journal of the American College of Medical
954 Genetics 19(12), Doi: 10.1038/gim.2017.107.
955 [68] Bapat, S.P., Whitty, C., Mowery, C.T., Liang, Y., Yoo, A., Jiang, Z., et al., 2022. Obesity alters
956 pathology and treatment response in inflammatory disease. Nature 604(7905): 337–42, Doi:
957 10.1038/s41586-022-04536-0.
958 [69] Parvaneh, N., Quartier, P., Rostami, P., Casanova, J.-L., de Lonlay, P., 2014. Inborn errors of
959 metabolism underlying primary immunodeficiencies. Journal of Clinical Immunology 34(7): 753–71,
960 Doi: 10.1007/s10875-014-0076-6.
961 [70] Bugge, A., Dib, L., Collins, S., 2014. Measuring respiratory activity of adipocytes and adipose tissues
962 in real time. Methods in Enzymology 538: 233–47, Doi: 10.1016/B978-0-12-800280-3.00013-X.
963 [71] Agilent Technologies., Seahorse XFp Cell Mito Stress Test Kit User Guide:
964 https://www.agilent.com/cs/library/usermanuals/public/XFp_Cell_Mito_Stress_Test_Kit_User_Gui
965 de.pdf, 18.
966 [72] Agilent Technologies., Seahorse XF Cell Energy Phenotype Test Kit User Guide:
967 https://www.agilent.com/cs/library/usermanuals/public/XF_Cell_Energy_Phenotype_Test_Kit_Us
968 er_Guide.pdf, 20.
969 [73] Agilent Technologies., Seahorse XF Glycolysis Stress Test Kit User Guide:
970 https://www.agilent.com/cs/library/usermanuals/public/XF_Glycolysis_Stress_Test_Kit_User_Gui
971 de.pdf, 22.